

Lattice dynamics of thin layers of molecular nitrogen adsorbed on graphite

S. E. Roosevelt* and L. W. Bruch

Department of Physics, University of Wisconsin—Madison, Madison, Wisconsin 53706

(Received 14 December 1989)

Monolayer and bilayer solid lattices of molecular nitrogen adsorbed on the basal plane surface of graphite are modeled with realistic intermolecular-potential models, and the Helmholtz free energy is evaluated with quasiharmonic lattice dynamics. The stability of herringbone and pinwheel orderings of the layers relative to each other and to the low-temperature three-dimensional solid is determined. There is good agreement with the observed length and energy scales of the monolayer and bilayer lattices. The modeling is consistent with the following succession of lattices: commensurate monolayer herringbone, uniaxially incommensurate monolayer herringbone, monolayer pinwheel, and bilayer pinwheel or bilayer uniaxially incommensurate herringbone.

I. INTRODUCTION

Molecular nitrogen adsorbed on the basal-plane surface of graphite, N_2 /graphite, is the molecular physical adsorption system for which the most detailed and most extensive body of experimental data exists. It displays several geometrical packings and ordering transitions and has already been the subject of much theoretical effort. We report here calculations which attempt, and to a considerable degree succeed in reaching, a quantitative account of the lengths and energies of the ordered monolayer and bilayer lattices based on molecular-interaction models.

The low-temperature solid of three-dimensional molecular nitrogen has the $Pa3$ structure of ordered molecular axes which often occurs for solids of linear molecules.^{1,2} This intricate ordering is disrupted, or frustrated, in the adsorbed monolayer and there is a limited layer-by-layer condensation at low temperatures.³ We treat the evolution of the ordering in monolayer and bilayer structures under an increasing mechanical stress which changes the relative importance of the intermolecular and molecule-substrate forces. As for three-dimensional solids of linear molecules,⁴ several orderings have comparable energies and the succession of phases under increasing stress depends on small stability margins.

The phase transitions of N_2 /graphite may be grouped roughly as thermally or mechanically driven. The thermally driven class includes orientational ordering and melting transitions, identified in thermodynamic experiments such as specific heat^{5–8} and adsorption isotherm measurements.⁹ The mechanically driven class includes commensurate-incommensurate and layer condensation transitions, for which structural information is obtained from diffraction experiments with electrons,¹⁰ neutrons,^{11–14} and x rays;^{15,16} there also are signatures in the thermodynamic experiments. The monolayer solid displays commensurate and uniaxially incommensurate rectangular lattices and a triangular incommensurate lattice; the structural assignment for the bilayer solid is still uncertain. We attempt to reproduce the observed succession of lattices with our model calculations.

The dense phases of molecular nitrogen are usually held to be governed by classical mechanics, although the quantum-mechanical zero-point energy^{17–19} is 15% of the cohesive energy of the low-temperature three-dimensional solid. The orientational ordering transition and fluid states of the adsorbed nitrogen have been treated^{20,21} with classical Monte Carlo and molecular-dynamics methods. Previous treatments^{22–24} of the relative stability of the low-temperature thin solid layers were based on potential-energy calculations or on Monte Carlo calculations applied at very low temperatures. We present here stability calculations for the ordered solids with the quasiharmonic lattice approximation²⁵ for the Helmholtz free energy; thus the lattice dilation caused by the zero-point energy is included. This is the first work in which the internal parameters of the molecular lattice are varied to minimize the quasiharmonic free energy; vibrational and librational spectra were calculated previously^{26–28} for specific structures of monolayer N_2 /graphite.

The organization of the paper is as follows. Section II contains definitions of the proposed lattices and unit cells for monolayer and bilayer solids, a description of the interaction models and a summary of the quasiharmonic theory. Section III contains a review of experimental data for adsorbed nitrogen and of previous theoretical treatments. The results of our calculations and a comparison to the experimental observations are presented in Sec. IV. Section V contains a final discussion.

II. FORMULATION

A. Lattices

We treat structures of the monolayer and bilayer solids of nitrogen based on the triangular and rectangular lattices, two-dimensional Bravais lattices of high symmetry. The triangular lattice with four and eight molecules in the bases for the monolayer and bilayer, respectively, has similarities to the $Pa3$ ordering² in three dimensions. The rectangular lattice with two- and four-molecule bases for the monolayer and bilayer, respectively, has the

geometry observed¹⁰ in the initial stages of the monolayer. Each (rigid) molecule has five coordinates (three for the center-of-mass position and two for the orientation of its axis), so that there are 10–40 variables per unit cell for these structures. Assuming pinwheel ordering for the triangular lattice cell and herringbone ordering for the rectangular cell imposes relations among the average coordinates. Although these assumptions limit the search for the optimal structures, rather high symmetry structures are in accord with overall features of the experimental observations.

The ordered low-temperature solid of nitrogen and of many other linear molecules has the $Pa3$ structure^{1,2} with a simple cubic primitive space lattice and a four-molecule basis. The molecular centers are sited at the corners and face centers of the cubic cell. Figure 1 shows a projection of three successive layers onto the (111) plane; these are the repeating sequence in the close-packed stack of triangular lattices in a face-centered-cubic lattice of a monatomic species.

The four-molecule basis in one of the (111) planes (Fig. 2) shows pinwheel ordering: one (“pin”) molecule has its axis perpendicular to the plane and three (“wheel”) molecules have axes which are related by successive 120° rotations about the (111) direction. The spherical polar coordinates of the molecular axes in the $Pa3$ lattice are set by the symmetry: for molecule “2” the polar angle is 109.47° (or 19.47° into the plane) and the azimuthal angle is 30° relative to the A_1 axis.

We take the unit cell in Fig. 2 as the basis of the pinwheel monolayer lattice. The spherical polar coordi-

nates of the wheel molecule “2” are internal coordinates to be determined by free-energy minimization. The axis vector of molecule “2” is expressed as

$$\hat{n}_2 = \cos\phi \cos\chi \hat{X} + \cos\phi \sin\chi \hat{Y} - \sin\phi \hat{Z}, \quad (2.1)$$

with Cartesian axes \hat{X} and \hat{Y} shown in Fig. 2 and the \hat{Z} axis directed outward from the substrate. The orientations of molecules “3” and “4” are obtained by successive 120° rotations of \hat{n}_2 about the (111) or \hat{Z} axis, as for the $Pa3$ lattice.

The unit cell of the pinwheel bilayer is constructed from the four-molecule cells of layers A and B , shown in Fig. 1. The angles ϕ and χ , defined as in Eq. (2.1), differ for the wheel molecules in the two layers. As shown in Fig. 1, the second layer is displaced laterally with respect to the first layer so that its pin molecule is in a site of threefold symmetry with three wheel molecules in the first layer as neighbors. The interlayer spacing is not simply related to the lateral spacings.

In both the monolayer and bilayer pinwheel lattices, the pin molecules may have a different center-of-mass distance from the substrate than the corresponding wheel molecules. The wheel molecules are physically equivalent; thus while the four molecules in the $Pa3$ basis are physically equivalent, the monolayer basis has two inequivalent molecules and the bilayer basis has four inequivalent molecules.

The planar herringbone lattice is defined with the rectangular unit cell and two sublattices shown in Fig. 3. Molecules “ B ” are centered in the rectangle formed by “ A ” molecules and the axial orientations are given by

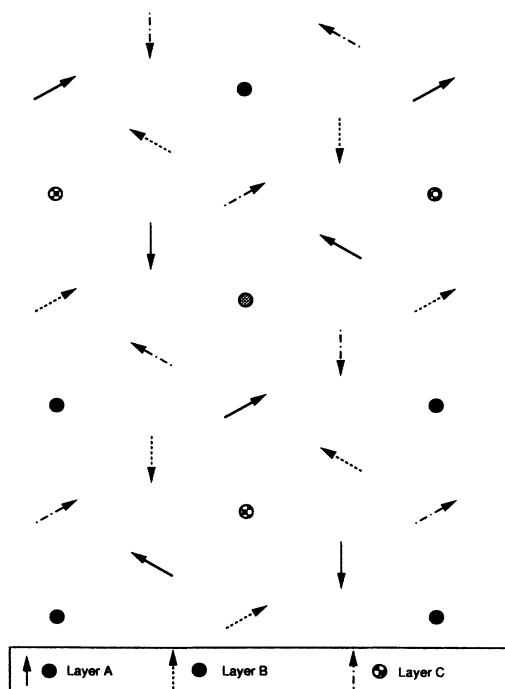


FIG. 1. Two-dimensional projection of layer stacking along the (111) axis of the $Pa3$ lattice. The stacking sequence is ABC . Circles denote molecular axes oriented perpendicular to the plane and arrows indicate the orientations of projections of molecular axes onto the plane.

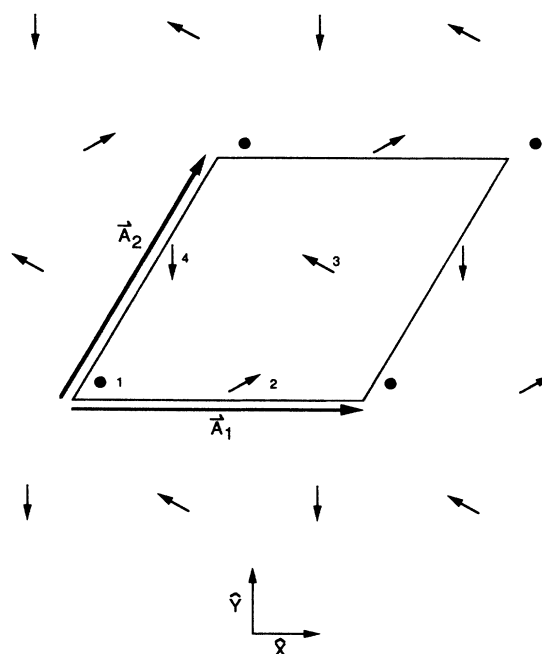


FIG. 2. Four-molecule unit cell in the (111) plane of the $Pa3$ lattice. X and Y axes and primitive vectors of the triangular Bravais lattice are shown. The four-molecule basis of the monolayer pinwheel, with the axis of molecule 1 perpendicular to the plane, is shown.

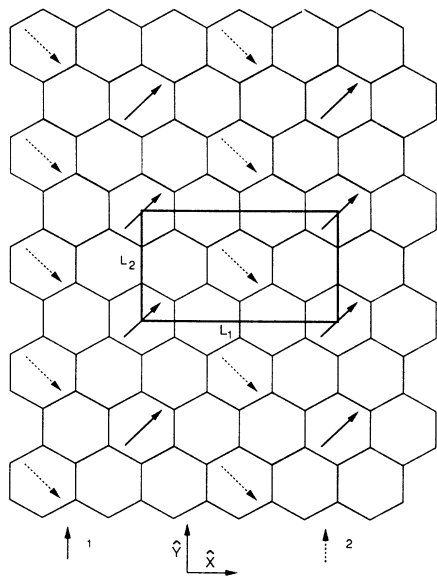


FIG. 3. Monolayer herringbone lattice showing unit cell and two sublattices. The background represents the basal-plane surface of graphite. This herringbone is in the commensurate $(\sqrt{3} \times \sqrt{3})R 30^\circ$ lattice; more general rectangular lattices with the same value of L_2 , but with $L_1 \neq L_2\sqrt{3}$, are termed uniaxially incommensurate lattices.

$$\hat{n}_A = \cos\phi \cos\chi \hat{X} + \cos\phi \sin\chi \hat{Y} - \sin\phi \hat{Z} \quad (2.2)$$

and

$$\hat{n}_B = \cos\phi \cos\chi \hat{X} - \cos\phi \sin\chi \hat{Y} - \sin\phi \hat{Z} ;$$

the molecules are at the same height from the substrate and are physically equivalent. The case $\phi=0$ is termed the “2-in herringbone” lattice; the case with $\phi \neq 0$ is termed the “2-out herringbone.”

The bilayer herringbone lattice is constructed from two planar herringbones, with spherical polar coordinates (ϕ_1, χ_1) and (ϕ_2, χ_2) for the first and second layers, respectively. The “A molecules” of the second layer are displaced from the A molecules of the first layer by $C_x L_1 \hat{X}$. We have also treated more general lateral positioning of the second layer but the energy minima still occurred for zero displacement along the \hat{Y} axis. There are two inequivalent molecules, one from each layer, in the four-molecule basis.

The bilayer herringbone lattices are closely related to two structures treated by James⁴ in his analysis of hexagonal-close-packed (hcp) stacks of linear molecules. The case in Fig. 4(a), in which ϕ_1 and ϕ_2 and also χ_1 and χ_2 have the same signs, is labeled the $P2_1/c$ structure by O’Shea and Klein.²⁹ The case in Fig. 4(b), ϕ_1 and ϕ_2 , and also χ_1 and χ_2 , have opposite signs, corresponds to the $Pca2_1$ structure.

The monolayer and bilayer herringbone lattices illustrated in Figs. 3 and 4 show the full registry of the $(\sqrt{3} \times \sqrt{3})R 30^\circ$ commensurate monolayer. We also treat two other classes of uniform herringbone lattices: (1) incommensurate lattices in which L_1 and L_2 have no sim-

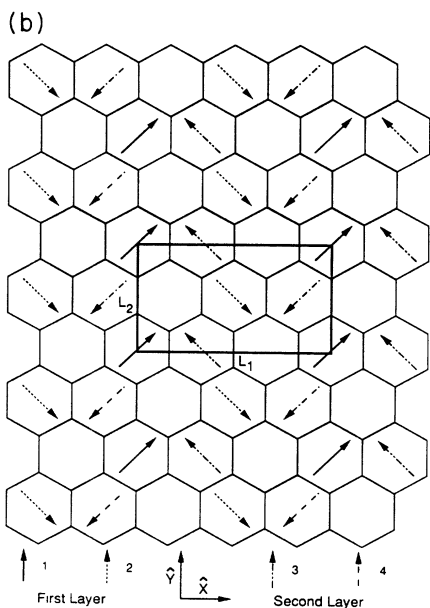
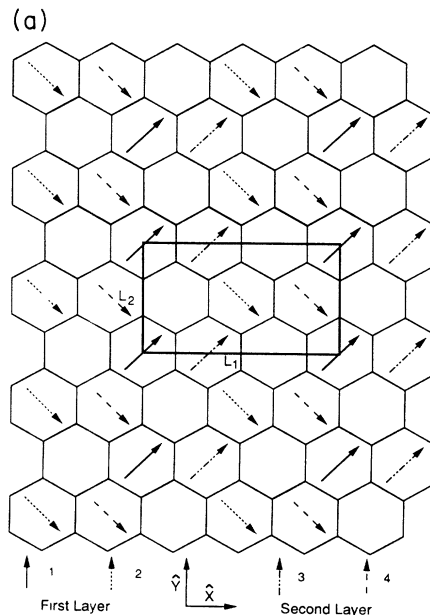


FIG. 4. Bilayer herringbone lattice showing unit cell with four sublattices. The background represents the basal-plane surface of graphite. In the text, the uniaxially incommensurate bilayer herringbone lattice is treated, in which L_2 remains at 4.26 Å and L_1 is varied. The positioning of molecule 3 along the x-axis, expressed as a distance $C_x L_1$ from molecule 1, is also an adjustable parameter. (a) $P2_1/c$, (b) $Pca2_1$.

ple relation to the substrate, and (2) uniaxial incommensurate lattices in which L_2 is held at the 4.26 Å value of the graphite and L_1 is permitted to have a continuous range of values. The number of molecules in the basis remains the same; there is no provision^{21,24} for modulation of the adlayer along the incommensurate axis by the periodic substrate potential. In comparisons of structural

stability, this approximation artificially enhances the periodic energy contributions for commensurate layers.^{21,24}

B. Interactions

The interaction model for the adsorbed nitrogen system is constructed similarly to those for adsorbed inert gases:³⁰ an intermolecular potential which reproduces three-dimensional solid data is supplemented by estimates of the substrate-mediated interactions and by a model for the interaction of the molecule with the substrate. The molecular case is made more complex³¹ by the anisotropy of the intermolecular potential and by the static multipole moments of the isolated molecule. However, quantum-chemistry calculations^{32,33} of the interaction and experimental data for librational frequencies³⁴ test the models of the anisotropy. We discuss here the components of two interaction models for which we made extensive calculations.

1. Atom-atom interaction models

The interaction of an isolated pair of nitrogen molecules is divided into an electrostatic energy arising from the static multipole moments and an energy analogous to the inert-gas potential energy. For the latter, we use a sum of spherically symmetric potentials with force centers at the nitrogen nuclei. Such atom-atom interaction models

$$\Phi = \sum_{i=1}^z \sum_{j=3}^4 \phi(r_{ij}) \quad (2.3)$$

were introduced as empirical models with rather simple functions for ϕ ; the calculations³² of Berns and van der Avoird have been fitted to this form too. Ling and Rigby³⁵ review the nitrogen atom-atom models.

Etters *et al.*³⁶ adjusted the potential of Berns and van der Avoird to fit the solid-nitrogen data better and gave as the functional dependence for $r > 3.45 \text{ \AA}$

$$\phi(r) = A \exp(-\alpha r) - B/r^6, \quad (2.4)$$

with $A = 9.261205 \times 10^7 \text{ K}$, $\alpha = 4.037 \text{ \AA}^{-1}$, $B = 1.79 \times 10^5 \text{ K \AA}^6$, and molecular internuclear spacing $l = 1.094 \text{ \AA}$. We take Eq. (2.4) as the "Etters model," although slightly smaller nitrogen atomic separations occur in the densest layers treated. Bulk-nitrogen properties for this model and slight variants of it have been reported.^{32,36,37,38} Kuchta and Etters^{23,24} applied it to $\text{N}_2/\text{graphite}$.

Our most extensive calculations are for the X1 model of Murthy *et al.*;³⁹ it has the Lennard-Jones (12-6) potential

$$\phi(r) = 4\epsilon[(\sigma/r)^{12} - (\sigma/r)^6] \quad (2.5)$$

for Eq. (2.3), with $\epsilon = 36.4 \text{ K}$, $\sigma = 3.318 \text{ \AA}$, and molecular internuclear spacing $l = 1.098 \text{ \AA}$. Murthy *et al.*^{39,40} reported bulk-nitrogen properties for this model. It has been applied in several calculations for $\text{N}_2/\text{graphite}$.^{22,28,41,42}

The pair-molecule energy sums omit multibody ener-

gies such as the triple-dipole dispersion energy. Monson and Rigby estimate⁴³ that the triple-dipole energy for three-dimensional (3D) solid nitrogen is less than 50 K in a total lattice potential energy of -1000 K . We neglect it.

2. Electrostatics

An isolated nitrogen molecule has a permanent quadrupole moment⁴⁴ of $-(1.42 \pm 0.08) \times 10^{-26} \text{ esu cm}^2$. However, at center-of-mass separations corresponding to nearest neighbors in the 3D solid, there is considerable interpenetration of the charge clouds of the nitrogen molecules.⁴⁵ Both to better represent the average charge distribution of the molecule and because the displacement expansions for the lattice dynamics are formed more easily, we use distributed point-charge representations for the electrostatic moments.

The Etters model³⁶ has a $4q$ representation: charges $0.373|e|$ are located along the internuclear axis at $\pm 0.847 \text{ \AA}$ from the center of mass and $-0.373|e|$ at $\pm 1.044 \text{ \AA}$ from the center of mass. The corresponding quadrupole moment is $-1.34 \times 10^{-26} \text{ esu cm}^2$.

The X1 model³⁹ has a $3q$ representation: charges $-0.405|e|$ are placed at the nuclear sites, $\pm 0.549 \text{ \AA}$ from the center of mass, and a charge $0.810|e|$ at the center of mass. This corresponds to a quadrupole moment $-1.173 \times 10^{-26} \text{ esu cm}^2$, which was shifted from the isolated molecule value as part of the fitting of the 3D dense phase data.

In spite of quite different point-charge representations in these models, the electrostatic energy for the lattices which we treat scales mostly as the square of the corresponding point quadrupole moments. The total electrostatic energy is rather insensitive to the details of the distributed charges.

3. Holding potential

Nitrogen is physisorbed to the basal-plane surface of graphite and Steele⁴⁶ modeled the holding potential in analogy to his constructions for inert gases adsorbed on graphite. The holding potential is a sum of spherically symmetric atom-atom pair potentials for the interaction between the atoms of the nitrogen molecule and the carbon atoms of the graphite substrate. Two functional forms are used for the nitrogen atom to substrate atom potential: the exponential -6 form of Eq. (2.4) and the Lennard-Jones (12-6) potential of Eq. (2.5).

Kuchta and Etters²³ give for the holding-potential parameters in Eq. (2.4) the values $A = 5.6537 \times 10^7 \text{ K}$, $B = 1.5976 \times 10^5 \text{ K \AA}^6$, and $\alpha = 3.8966 \text{ \AA}^{-1}$, with a triangular Bravais cell of side 2.46 \AA for the graphite and an interlayer spacing of 3.357 \AA . We take as the holding-potential parameters for Eq. (2.5), to go with the X1 model, $\epsilon = 31 \text{ K}$ and $\sigma = 3.36 \text{ \AA}$, with a Bravais cell of side 2.46 \AA and an interlayer spacing of 3.37 \AA ; slightly different values are used with the X1 model by other workers.^{28,42}

In the Fourier decomposition⁴⁷ of the net holding potential into a laterally averaged term and terms with la-

teral periodicity expressed in terms of the reciprocal-lattice vectors of the surface triangular lattice, we retain only the first nonzero shell of reciprocal-lattice vectors. The lateral average potential has a sum over 15 planes of carbon atoms, while only the first carbon plane is used for computing the first Fourier amplitude.

These holding potential models have similar values, about -1100 K, for the lateral average energy minimum of N_2 on graphite. In spite of the different functional forms of the repulsions, the lateral variation of the holding potential at an overlayer spacing corresponding to the potential minimum is also quite similar.

When the electrostatic screening of the nitrogen quadrupole moments by the substrate is included in the effective interactions among the nitrogen molecules, the corresponding term²² is included in the holding potential and contributes about -30 K.

Joshi and Tildesley⁴⁸ modified the holding-potential construction to include terms reflecting the dielectric anisotropy of the graphite. The lateral average of the holding potential is not affected by their modification, but the leading Fourier components have increased amplitudes. Commensurate and partially commensurate lattices would have greater stability with the modified holding potential, but it was not used in this work, which already has some drastic approximations for the uniaxial incommensurate monolayer.

4. Substrate-mediated interactions

Two adsorption-induced interactions are frequently included in the energy calculations for adsorbed inert gases:³⁰ (1) the effect of substrate screening of the electric fields of static moments on the adsorbate, represented by electrostatic images, and (2) the effect of the dynamic screening response of the substrate to fluctuating dipole moments on the adsorbate in reducing the intermolecular van der Waals energy, the McLachlan interaction.⁴⁹ We include these terms in the static potential energy of the adsorbed nitrogen.

The electrostatic image energy has the same prescription as used before for linear molecules:²² the reference plane for the image is located at

$$z_I = z - d/2, \quad (2.6)$$

where z is the distance of the molecular center of mass from the outermost plane of carbon atoms in the graphite and d is the interlayer spacing of the graphite. The image energy is not included in all the calculations. As discussed in Sec. IV B, there are some lattice instabilities which we consider to be artifacts of the modeling. Belak *et al.*⁵⁰ and Peters and Klein⁵¹ also noted problems arising from the use of this prescription for the static screening response for carbon monoxide adsorbed on graphite.

We construct the coefficients in the McLachlan interaction from the data of Rauber *et al.*,⁵² $C_{s1} = 33.4$ a.u. and $C_{s2} = 17.0$ a.u., and use Eq. (2.6) for the distance to the image plane. Thus a spherical-average approximation is used for the nitrogen molecules. Kim *et al.*⁵³ report the generalization of the McLachlan interaction for linear molecules. We made trial calculations for the her-

ringbone monolayer, approximating the molecular polarizability anisotropy by its static value.⁵⁴ The energy shifts were only of the order of 15% of the spherical-average McLachlan term, and the anisotropy was omitted for the calculations reported here. Kuchta and Etters²³ incorporated some molecular anisotropy in their calculations by distributing the McLachlan coefficients, calculated in the spherical approximation, over the four pairs in an atom-atom representation of the intermolecular potential.

We truncate all components of the intermolecular potentials for molecular center-of-mass separations equal to 33.18 Å, i.e., ten times the σ of the $X1$ potential; contributions to the static potential energy and to the dynamical matrix for molecules at larger separations are omitted.

C. Static and quasiharmonic energies

The total potential energy for the array of nitrogen molecules is the sum of the terms described in Sec. II B:

$$\Phi = V_{\text{pair}} + V_{\text{quad}} + V_{\text{image}} + V_{\text{McL}} + V_{\text{hold}}, \quad (2.7)$$

the atom-atom (pair), distributed point charge (quadrupole), static substrate screening (image), McLachlan (McL), and holding potentials. We made parallel calculations incorporating or omitting the electrostatic image terms and using the $X1$ model³⁹ or the Kuchta-Etters model.²³

The frequencies for small-amplitude oscillations of the molecules about an average lattice are derived from the dynamical matrix constructed by a small displacement expansion of the potential energy defined in Eq. (2.7). More precisely, we do not include the V_{image} and V_{McL} terms in the expansion procedure; we include V_{quad} because we found unstable dynamics for the commensurate herringbone lattice when it was omitted. The expansion⁵⁵ to generate the dynamical matrix is straightforward but tedious because of the number of sublattices to be included. The size of the hermitian dynamical matrix ranges from 10×10 for the monolayer herringbone to 40×40 for the bilayer pinwheel. The frequencies, for each wave vector, are determined with standard numerical eigenvalue methods, but the calculations with many polarizations are lengthy and the eigenvectors reflect mixing of many coordinates.

The Helmholtz free energy at temperature T is, in the quasiharmonic approximation,

$$F = \Phi + k_B T \sum_{k,\lambda} \ln[2 \sinh(\hbar\omega_{k,\lambda}/2k_B T)], \quad (2.8)$$

where Φ is the static potential energy [Eq. (2.7)], k_B is Boltzmann's constant, \hbar is the reduced Planck constant, and $\omega_{k,\lambda}$ are the angular frequencies for wave vector k and polarization index λ . The sum extends over all polarizations and over wave vectors in the first Brillouin zone. At zero temperature the free energy is equal to the internal energy, which is the sum of the static potential energy and the zero-point energy

$$E_0 = \Phi + \sum_{k,\lambda} (\hbar\omega_{k,\lambda}/2). \quad (2.9)$$

The free energy per molecule $f = F/N$ is minimized with respect to variations of the internal structural parameters, as in calculations for bilayers and trilayers of inert gases.^{25,56} The spreading pressure p is then the isothermal derivative of the free energy f with respect to the area per molecule a ,

$$p = - \left(\frac{df}{da} \right)_T, \quad (2.10)$$

and the chemical potential is

$$\mu = f + ap. \quad (2.11)$$

At zero temperature the chemical potential is equal to the enthalpy per molecule.

The normal-mode frequencies $\omega_{k,\lambda}$ and eigenvectors $e_{k,\lambda}$ also lead to mean-square vibration amplitudes, as follows. If j labels a Bravais cell, α the molecule in the basis, and β the component of the displacement (in the center of mass or angle), the corresponding mean-square displacement is

$$\langle (u_{j,\alpha;\beta})^2 \rangle = \sum_{k,\lambda} (\hbar/2N_B M \omega_{k,\lambda}) |e_{k,\lambda;\alpha;\beta}|^2 \times \coth(\hbar\omega_{k,\lambda}/2k_B T), \quad (2.12)$$

where M is the mass of molecular nitrogen, and N_B is the number of Bravais cells in the lattice. The fourth and fifth components of $u_{j,\alpha}$ are the angle increments scaled by $l/2$. The Goodings-Henkelman result¹⁷ for the mean-square deviation of the molecular axis is recovered from Eq. (2.12) by neglecting the coupling of the librations to the vibrations and the dispersion of the librational frequencies.

Relative stability of structures is decided by comparing values of μ at the same spreading pressure and temperature. The slope of an isotherm of μ as a function of p is the area a , so that the monolayer and bilayer lines have easily located crossings. Extrapolating to locate the transitions between monolayer phases with areas per molecule differing by 10–20% is delicate, because the slopes of the intersecting lines differ by only 10–20%.

The sum over wave vectors in the first Brillouin zone in Eqs. (2.8) and (2.9) is done with special points summations^{57,58} which are modified to reflect the symmetries of the normal-mode problem for a Bravais lattice with a molecular basis.⁵⁹

The minimum-energy or minimum-free-energy configuration as a function of area is determined by an iterative search for the optimal structural parameters. Essentially, searches are made on three-parameter grids, fitting calculations to a quadratic form and using the extrapolated minimum as the starting point of the next iteration. The 2-in monolayer herringbone has two parameters, the overlayer height and the planar herringbone angle χ (Fig. 3). While the 2-out herringbone is a possible result of the search, the optimal tip angle is zero for the molecular densities in this work. The monolayer pinwheel has four parameters, the overlayer heights to the pin and wheel molecules and two spherical polar coordinates for the orientation of the wheel molecule

axes. However, since the optimal tip angle of the monolayer wheel molecules is zero, this optimization effectively is in three variables. The herringbone bilayer has seven parameters: the overlayer height and spherical polar coordinates for the molecular axes in each layer, and the lateral offset $C_x L_1$ of the second layer. The optimization for the herringbone bilayer is an iteration of three parameter searches within each layer, for given C_x , followed by a variation of C_x . The bilayer pinwheel has eight parameters, four for each layer. This optimization is an iteration of three parameter searches for specified azimuthal angles of the two layers, followed by a search in χ_1 and χ_2 . Implementing such searches requires an efficient energy calculation for a given configuration.

III. REVIEW

A. Experimental data for low-temperature N_2 /graphite

We summarize information on orientationally ordered bulk and thin-layer phases of molecular nitrogen at low temperatures. The molecular centers of mass are arranged on regular lattices and the molecular axes too have a spatial periodicity. Data for the bulk α - N_2 solid⁶⁰ and for low-coverage nitrogen adsorbed on graphite were used in constructing the molecule-molecule potential and the molecule-graphite potential; in the analysis of the adsorbed layers, they provide comparison energy and length scales. The data for the thin ordered layers of nitrogen adsorbed on the basal-plane surface of graphite, N_2 /graphite, set the framework for the discussion of our calculations.

We emphasize thermodynamic paths of increasing chemical potential at constant temperature, corresponding to an increase of mechanical stress. The monolayer condenses^{10,12,15} in the commensurate $(\sqrt{3} \times \sqrt{3})R 30^\circ$ lattice and under increasing 3D gas pressure makes transitions to uniaxial incommensurate^{61,62} and then to triangular incommensurate^{10,63} monolayer lattices. With further increase, the bilayer condenses^{10,14,64} and then the bulk solid; apparently there is a limited layer-by-layer growth at low temperatures.³

Other interesting thermodynamic paths are for increasing temperature at approximately constant chemical potential. Such paths display^{5–8} orientational disordering transitions at temperatures in the range 25–35 K and melting transitions. The quasiharmonic lattice theory, however, is not applicable to these phenomena and we do not consider them further.

The ground state of the 3D α - N_2 has cohesive energy -831 K/molecule (Ref. 18) for nearest-neighbor spacing 3.994 Å of the molecular centers of mass.⁶⁰ The lattice potential energy¹⁸ is -1002 ± 25 K. The zero-point energy is given as 156 K by Goodings and Henkelman,¹⁷ from measured vibration and libration frequencies, and as 160 K by LeSar.⁶⁵ The molecular axes have the ordering of the $Pa3$ structure (Sec. II A and Fig. 1).

The isosteric heat for N_2 /graphite at very low coverage is reported to be 10.1 ± 0.2 kJ/mole at 90–210 K (Ref. 66) and 10.4 ± 0.1 kJ/mole at 80 K.⁶⁷ Since thermal energy terms of the adsorbed and 3D gases nearly cancel,²²

the minimum potential energy for one nitrogen molecule interacting with the basal-plane surface of graphite is -1170 to -1250 K.

The $(\sqrt{3} \times \sqrt{3})R 30^\circ$ monolayer lattice has herringbone ordering of the molecular axes at temperatures below 28 K.^{61,11,15} The heat of adsorption q_1 at the condensation is 1260–1290 K/molecule, from data at temperatures in the range 45–55 K.⁶⁴ The nearest-neighbor spacing on the triangular lattice of molecular centers is 4.26 Å. The 2-in herringbone ordering is inferred from the presence of a superlattice diffraction peak in neutron scattering¹² and from glide-plane symmetries corresponding to the extinction of leading superlattice peaks.⁶¹ The angle χ is $45^\circ \pm 5^\circ$, from fits to neutron-diffraction intensities.¹³

Under isothermal compression, the commensurate monolayer is succeeded by a uniaxially incommensurate monolayer lattice with observed misfits along the long (“x”) axis of the herringbone cell of 2–5%.⁶² At very low temperatures, the commensurate-to-incommensurate transition may be discontinuous.⁸ The uniaxial incommensurate lattice has 2-in herringbone ordering, according to glide-plane symmetries reflected in low-energy electron diffraction (LEED) patterns.^{10,61} From an adsorption isotherm⁶⁸ at 34.3 K we estimate that a chemical-potential increase of at least 200 K from the condensation value is needed to drive the adlayer to 5% uniaxial misfit.

Under further compression, the monolayer forms an incommensurate lattice which, to 1%, has a triangular arrangement of the molecular centers of mass.⁶³ Low-energy electron diffraction experiments show lattices with nearest-center spacings in the range 4.15–4.04 Å.^{10,62} The nearest-center spacing in the densest monolayer is about 4.04 Å in both LEED (Ref. 63) and neutron diffraction.^{12,14} You and Fain⁶³ identify the orientational ordering as a “2-out herringbone,” on the basis of an apparent glide-plane extinction of a leading diffraction peak; Wang *et al.*¹⁴ identify it as a four-sublattice pinwheel, on the basis of intensity analysis of neutron-diffraction data.

The bilayer solid at low temperatures has a double-period superlattice (relative to the center-of-mass lattice) with no glide-plane symmetries apparent in the LEED data.¹⁰ The 2D center-of-mass lattice is nearly triangular, with a small obliquity and an area of 14.1 Å² per molecule in each layer, according to the analysis of the neutron-diffraction data.¹⁴ The data were fitted to both pinwheel and 2-out herringbone models. The chemical potential at the bilayer condensation can be estimated from the second-layer risers in LEED isotherms:⁶⁴ it is about 80 K lower than the value for what was identified as fourth-layer condensation and which we take as essentially the bulk chemical potential.⁶⁹

B. Modeling of N₂/graphite

There have been two types of theoretical treatment of the phenomena observed in thin layers of N₂/graphite: (1) analysis of the ordering of the molecular axes in terms of the phases of point quadrupoles arranged on a rigid triangular lattice,^{29,70–72} and (2) calculation^{20–24,41,42,73,74}

of structures, thermal averages, and time correlations with intermolecular potential models. The first of these contributes an overview of the phase diagrams and the language (2-in herringbone, 2-out herringbone, and pinwheel) which is used to describe the orientational ordering. The second attempts to clarify the succession of observed lattices and to place the phenomena of this system in a wider perspective of solids of linear molecules.^{51,75} We review the theoretical work to set the background for the present calculations.

Harris and Berlinsky⁷⁰ gave a mean-field approximation for the statistical mechanics of a monolayer of point quadrupoles on a rigid triangular lattice with nearest-neighbor interactions. They determined the stabilities of various orderings as a function of the temperature and of the ratio of the quadrupole-quadrupole interaction to an aligning crystal field of the underlying substrate. The ground state of the 2-in herringbone has a planar angle χ (Fig. 3) equal to 45° . The angles for the ground state of the pinwheel structure, Fig. 2, are $\phi=0^\circ$ and $\chi=38.81^\circ$, compared to values 19.47° and 30° in the close-packed plane of the *Pa3* lattice. The angle χ for the monolayer pinwheel depends on the range used for the quadrupole interaction; we find that when many shells of neighbors are included, it increases from 38.81° to 39.5° .

O’Shea and Klein²⁹ determined the lowest-energy orderings of several bilayer arrays of point quadrupoles on rigid triangular lattices. These include pinwheel and 2-out herringbone orderings. The bilayer pinwheel case is an intermediate state between the monolayer and bulk pinwheel lattices: for the “free bilayer” (no external potential), the optimal angles for nearest-neighbor point quadrupole interactions are $\phi=10.49^\circ$ and $\chi=34.90^\circ$; extending the interaction to many neighbor shells we find the optimal angles become $\phi=12.3^\circ$ and $\chi=35.0^\circ$. These values show the beginning of the healing of the frustrated ordering in the monolayer toward the bulk 3D solid order.

In related work, Kobashi and Eters⁷⁶ determined the relaxations of the outermost layers at the (111) surface of α -N₂, with a realistic intermolecular potential. The first layer has a slightly distorted pinwheel basis; the angles are $\phi=23.4 \pm 0.2^\circ$ and $\chi=32.0 \pm 0.1^\circ$.

The simplest treatments based on intermolecular potentials are potential-energy minimizations to find the lowest-energy configuration as a function of area/molecule.^{26,22,23} Such calculations are directed at deciding the optimal orientation (e.g., the herringbone angle) in a type of lattice and the relative stability of different lattice types. Since the zero-point energy in the nitrogen lattices is about 15% of the potential energy, conclusions based on stability margins of tens of kelvins in chemical potential, as occur in the calculations, have to be accepted cautiously.

A direct extension of the potential-energy minimization work is to treat excitations of the lattice by small-amplitude oscillation theory, termed quasiharmonic lattice dynamics.^{25,55} The frequency spectrum for the $(\sqrt{3} \times \sqrt{3})R 30^\circ$ herringbone monolayer was first calculated by Fuselier *et al.*;²⁶ the adlayer frequency gap at the Brillouin-zone center is now measured by inelastic

neutron scattering.⁷⁷ Cardini and O'Shea²⁷ calculated and extensively discussed the frequency spectra for herringbone monolayers; the harmonic phonon frequencies agree well with peaks in molecular dynamics spectra up to 17 K, although anharmonic effects are apparent in the broadening of the molecular-dynamics spectra.⁷⁸

Monte Carlo simulations are used^{21,23,24} to treat the orientational disordering transition near 30 K in the adsorbed layer and to optimize structure without the biases imposed by the assumption of small unit cells in work such as the present paper. The uniaxial incommensurate herringbone monolayer constructed in this way shows local strong modulations ("stripes") at small misfits and a lattice with a nearly uniform rectangular cell for misfits larger than 5%.²⁴ The bilayer structures of Kuchta and Eters vary with lattice constant from bilayer herringbone to pinwheel atop a herringbone to bilayer pinwheel.²³

Molecular-dynamics simulations are used²⁰ to explore orientational ordering, time correlations, and the time development of motions in the adsorbed layers. The general structures usually are set by the initial conditions, but spontaneous rearrangement of seriously unstable configurations is seen.⁴² Vernov and Steele⁴² treated two uniaxial incommensurate bilayer films with herringbone ordering at 25 K which remained stable during the simulation. More recently, Bhethanabotla and Steele⁴² treated several dense-film cases, including triangular monolayer lattices, which show evidence of pinwheel structures; in the bilayer triangular lattices, there is nearly no evidence for pin molecules in the first layer. Tildesley and Lynden-Bell²⁸ studied the spectra of orientationally ordered and disordered monolayers; with quasiharmonic lattice dynamics for the vibrational and librational frequencies of the ordered layers, we find, as had Cardini and O'Shea,^{28,78} good agreement to the molecular-dynamics spectra for temperatures near 15 K.

Monte Carlo and molecular-dynamics simulations are based on classical mechanics, with no simple method of incorporating zero-point energies. Further, it is quite burdensome to construct thermodynamic free energies for stability analyses by these methods. The quasiharmonic theory includes zero-point energy effects and directly gives absolute free energies. Although it entails repetitious calculations of frequency spectra as a function of structural parameters and has biases introduced at the outset by the use of rather small unit cells, the quasiharmonic theory retains some advantages for treating orientationally ordered lattices of nitrogen.

IV. MONOLAYER AND BILAYER STRUCTURES

We determined the sequence of structures for both the X1 and the Eters models,^{39,23} with and without the electrostatic screening (image) terms^{22,30} for the permanent quadrupole moments and in both the static-lattice and harmonic-lattice approximations; i.e., there were eight parallel calculations. For a given interaction model (pair potential with specified substrate screening response), the sequence of structures is the same for the static- and

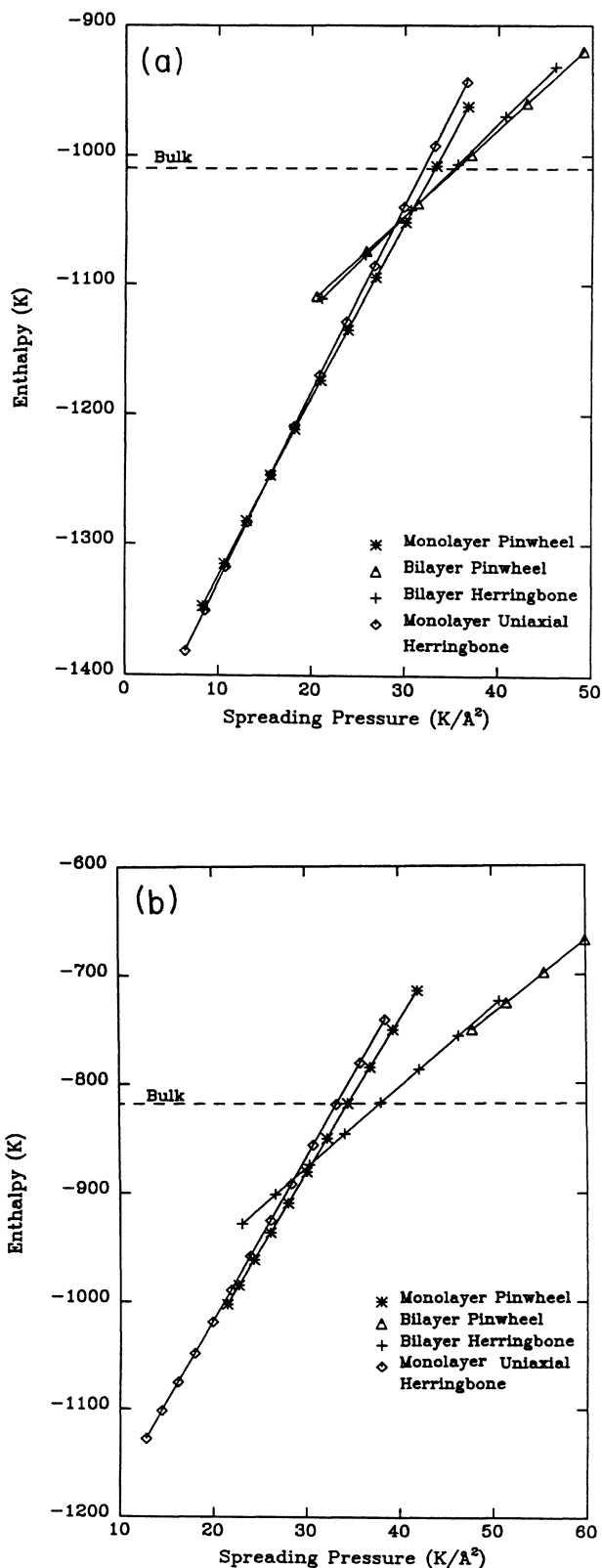


FIG. 5. Zero-temperature chemical potential (enthalpy) in K vs spreading pressure in $K/\text{\AA}^2$ for several monolayer and bilayer lattices of N_2 /graphite, with the X1 model including images. (a) static-lattice calculations, (b) harmonic-lattice calculations.

TABLE I. Succession of lattices of N_2 /graphite at zero temperature (see footnotes a and b).

Model	S	A >	μ	A <	S	A >	μ	A <	S	A >	μ	A <	S
X1—no image: static	MH	14.68	-1253	13.68	MP	13.41	-1040	7.19	BH	7.19	-1039	6.66	BP
	BP	6.64	-1010 ^c		Pa3								
	MH	15.28	-1111	14.49*	MP	14.01	-871	7.38	BH	7.35	-829	6.96*	BP
	BP	6.95*	-818 ^c		Pa3								
X1—no image: static	MH	14.47	-1093	13.51	MP	13.46	-1051	7.19	BH	7.17	-1010 ^c		Pa3
	MH	14.94	-928	14.15	MP	14.06	-881	7.39	BH	7.34	-818 ^c		Pa3
Etters—image: static	MH	14.72	-1183	13.78	MP	13.66	-1076	7.25	BH	7.22	-1031 ^c		Pa3
	MH	15.34	-1108	14.71*	MP	14.28*	-887	7.44	BH	7.41	-839 ^c		Pa3
Etters—no image: static	MH	14.61	-1081	7.25	BH	7.22	-1031 ^c		Pa3				
	MH	15.02	-900	7.45	BH	7.41	-839 ^c		Pa3				

^aS labels lattices at coexistence: MH = uniaxially incommensurate monolayer herringbone, MP = monolayer pinwheel, BH = uniaxially incommensurate bilayer $P2_1/c$ herringbone, BP = bilayer pinwheel, Pa3 = bulk 3D lattice.

^bAreas per molecule (in \AA^2) and chemical potential (in K) of coexisting phases. An asterisk denotes values obtained by extrapolation of pinwheel structure.

^cCoexistence condition for bulk. The possible occurrence of stable trilayers is not excluded by this work.

harmonic-lattice approximations. The zero-temperature chemical potential and areas per molecule at each phase coexistence are given in Table I. Figure 5 illustrates the locating of phase coexistences by intersections of chemical potential versus spreading pressure plots for the $X1$ model with images. We describe the structures for the $X1$ model with images in Sec. IV A and indicate the changes for the other cases; extensive tabulations are given elsewhere.⁵⁹ Some of the phase-transition determinations are based on extrapolations of the calculations; there are dynamical instabilities of the pinwheel lattices at large area per molecule and of the bilayer herringbone at small area per molecule, which we discuss in Sec. IV B.

A. Calculations

1. Bulk ($Pa3$) α - N_2

For internal consistency, we repeated calculations^{36,39,40} for the bulk structure. For the $X1$ model, the static potential energy is minimum, -1009.8 K/molecule, at the cubic lattice constant $L = 5.532$ Å and the harmonic cohesive energy (zero-point energy included) is minimum, -818.2 K, at $L = 5.66$ Å. The corresponding values for the Eters model are static minimum, -1030.5 K at $L = 5.59$ Å, and harmonic minimum, -839.2 K at $L = 5.70$ Å.

The harmonic zero-point energy 174 K for the $X1$ model agrees well with the value of Cardini and O'Shea⁷⁸ for a very similar model, but it is 10% larger than the empirical value of Goodings and Henkelman.¹⁷

The libration frequencies at the Γ point (Brillouin-zone center) for the Eters model at $L = 5.70$ Å, in the harmonic approximation, are 54.6, 67.1, and 100.3 K, a few percent lower than the values for the $X1$ model at its minimum.

2. Commensurate herringbone monolayer

The $(\sqrt{3} \times \sqrt{3})R30^\circ$ 2-in herringbone monolayer (Fig. 3) is the lowest-energy monolayer lattice, within our approximations, for each of the eight cases. For the $X1$ model with images, the static-energy minimum is -1483 K/molecule and the harmonic-energy minimum is -1335 K/molecule, both with a herringbone angle $\chi = 45.3^\circ$. The molecules are 3.31 Å above the graphite at the static minimum and 3.37 Å at the harmonic minimum. Without the image terms, the energies are about 20 K smaller in magnitude; most of the change arises in the single-molecule holding potential. The harmonic-energy minimum for the Eters model with images is -1320 K/molecule, with $\chi = 46.1^\circ$ and height 3.39 Å.

The monolayer heat of condensation at 50 K is 1260–1290 K/molecule, for a lattice which is orientationally disordered.⁶⁴ It is in fair agreement with the ground-state energy, considering the difference in the orientational states and the accumulated uncertainty in the total energy from the components of the models.

3. Uniaxial incommensurate herringbone and pinwheel monolayer phases

The harmonic ground-state energy of the commensurate monolayer is 5–10 K/molecule lower than the lowest energy state of the uniform uniaxial incommensurate monolayer for these models. The monolayer herringbones have zero-tilt angles (i.e., “2-in” configurations) even up to number densities for which the chemical potential is 400–500 K greater than the threshold for condensation of α - N_2 . This generalizes the finding of Peters and Klein⁷⁹ on the absence of 2-out monolayer herringbones, by including zero-point energy effects. Including the zero-point energy helps to stabilize the commensurate lattice: the minimum-energy uniform uniaxially incommensurate lattice has L_1 within 1% of 7.38 Å, while it is 4% smaller for the static potential-energy minimum.

The quadrupole interactions are essential for the dynamical stability of the monolayer herringbone lattice of N_2 /graphite. In early calculations for the commensurate monolayer and for the uniaxial incommensurate monolayer at small misfit, we found dynamical instabilities for the $X1$ model when the quadrupole terms were omitted from the dynamical matrix.

The existence of a range of chemical potential for which there is a stable monolayer pinwheel lattice depends sensitively on the interaction model. For the $X1$ potential, the chemical-potential range is 220 K when the image terms are included, but only 45 K when they are omitted. For the Eters model, with the image terms included the range is only about 110 K and the phase is absent when they are omitted.

In spite of drastically different division of energy into molecule-molecule and molecule-substrate potential energy for the herringbone and pinwheel lattices, the minimum potential energies for the structures are nearly equal. For the $X1$ potential with images, the minimum static potential energy of the herringbone is -1483 K/molecule, and that of the pinwheel (at molecular center spacing of 4.03 Å) is -1463 K/molecule. The center of the pin molecule is about 0.4 Å farther from the substrate than for the wheel molecules for most of the pinwheel lattices, and the azimuthal angle χ is in the range 36° – 38° .

When the calculations do yield stable monolayer pinwheels, the densest monolayer pinwheel occurs at second-layer condensation. The smallest separation of molecular centers is 3.94 Å in the $X1$ statics calculations and about 4.02 Å in the $X1$ harmonic-lattice calculations. As in other cases, the corresponding lengths for the Eters model are about 1% larger.

Uniaxial compression of the monolayer herringbone lattice is limited by the transition to the monolayer pinwheel or ultimately to the bilayer. For the $X1$ model harmonic-lattice calculations, the limit of L_1 compression set by the pinwheel is 3% at a chemical-potential increase of 220 K from the commensurate lattice (with image terms) and 5% at a chemical-potential increase of 390 K from the commensurate lattice (without image terms). In the former case, the limit set by the bilayer condensation is 5.5% at 450 K increase. In the Eters model

without images, to compress the herringbone by 4.5% requires more than a 400 K increase in the harmonic chemical potential; with images an increase of 210 K leads to 2.4% compression. The maximum compressions are of the order observed in diffraction experiments, but the chemical-potential increases⁶⁸ are much larger than the estimate of 200 K given in Sec. III A.

Properties of the monolayer pinwheel at areas greater than $14.3 \text{ \AA}^2/\text{molecule}$ for the $X1$ model with images and $14.35 \text{ \AA}^2/\text{molecule}$ for the $X1$ model without images are obtained by extrapolation. A direct search for minima of the quasiharmonic free energy at larger area leads to configurations with negative eigenvalues for the dynamical matrix (imaginary frequencies), which are correlated to unstable motions of the pin molecule for wave vectors near the center of the Brillouin zone.

The monolayer pinwheel configuration of minimum energy in all cases, $13.30\text{--}14.35 \text{ \AA}^2/\text{molecule}$, has zero-tilt angle for the wheel molecules, the $P6_3/m$ arrangement of the hcp stacking of linear molecules. The center of mass of the wheel molecules is 3.34 \AA above the graphite in the static lattice and 3.39 \AA in the harmonic lattice, for the $X1$ model with images; without image terms the values are 0.02 \AA larger, and for the Etters model the corresponding values are 0.02 \AA larger again.

4. Bilayer pinwheel and uniaxial incommensurate herringbone lattices

We treated five candidate bilayer lattices which, for a given interaction model, have closely spaced chemical potential versus spreading pressure plots: the bilayer pinwheel (Fig. 1), the uniaxial incommensurate herringbone $P2_1/c$ [Fig. 4(a)] and $Pca2_1$ [Fig. 4(b)] configurations and the same configurations of the completely incommensurate herringbone lattice. The multiplicity of herringbone orderings was explored because of reports^{10,18} that the bilayer $N_2/\text{graphite}$ has a nearly triangular center-of-mass lattice. If so, the aspect ratio L_1/L_2 of the herringbone unit cell should be close to $\sqrt{3}$ ($=1.732$). The ratio for the optimized bilayer herringbone lattices is in the range $1.55\text{--}1.62$ for the static lattice and $1.59\text{--}1.65$ for the harmonic lattice; dense herringbone packing of linear molecules appears to lead inevitably to aspect ratios much different from $\sqrt{3}$. Our most detailed studies are for the pinwheel and the uniaxial incommensurate $P2_1/c$ herringbone. The difference in chemical potential for other herringbone cases at the same spreading pressure is less than 5 K and the registry potential for the case we treated is less than 2 K/molecule, so that we do not have a conclusive assignment for the optimal bilayer herringbone lattice.

For the $X1$ model with images, we determined the optimal pinwheel configurations for areas per molecule in the ranges $6.575\text{--}6.725 \text{ \AA}^2$ (static lattice) and $6.75\text{--}6.90 \text{ \AA}^2$ (harmonic lattice). Beyond the largest areas for the harmonic lattice there is a dynamical instability at small wave vectors, which is associated with unstable motion of the second-layer pin molecule. The azimuthal angles χ are nearly equal in the two layers and are about 33° , with an increase of 0.5° over the range of areas. When the im-

age terms are omitted, the azimuthal angles in the first layer are about 1.5° larger than in the second layer. The tip angles ϕ (into the plane) are about 7° and 25° for the first and second layers, respectively, for the static lattice, and 7° and 24° for the harmonic lattice. While the center of mass of the first-layer pin molecule is 0.3 \AA higher than for its neighboring wheel molecules, the center of mass of the second-layer pin molecule is $0.03\text{--}0.06 \text{ \AA}$ lower than for its neighbors. The ratio of the interlayer spacing of the wheel molecules to the lateral spacing of the molecular centers is $0.84\text{--}0.87$, 5% larger than the ratio 0.816 for the $Pa3$ lattice. While there are many detailed differences, the overall trend is that the ordering in the bilayer pinwheel lattice is healing rapidly from the $P6_3/m$ ordering of the monolayer pinwheel toward the $Pa3$ order.

The internal parameters of the uniaxial incommensurate bilayer herringbone were optimized for areas/molecule of $7.05\text{--}7.3 \text{ \AA}^2$ for the static lattice and $7.2\text{--}7.5 \text{ \AA}^2$ for the harmonic lattice, for the $X1$ model with images, with similar ranges for the other cases. The lateral offset of the second layer, $C_x L_1$, has values of C_x close to 0.31 . The herringbone angle χ for the second layer is $0.5^\circ\text{--}1^\circ$ larger than for the first layer; the first-layer angle ranges from 53.5° to 50.0° for the static lattice and from 53.0° to 48.6° for the harmonic lattice. The tilt angles ϕ are 5° and 16° , into the plane, for the first and second layers, respectively, of the static lattice at $7.2 \text{ \AA}^2/\text{molecule}$; the values are 5° and 22° for the harmonic lattice at $7.35 \text{ \AA}^2/\text{molecule}$.

Only for the $X1$ model with image terms do we find a stable range for the bilayer pinwheel; the existence for the harmonic lattice is inferred by extrapolation. Without the image terms, the pinwheel has 8 K higher chemical potential than the bilayer herringbone at spreading pressures near the bilayer condensation. For the Etters model, the corresponding increment is $14\text{--}20 \text{ K}$. More thorough searches of the other bilayer herringbone configurations could only increase the stability margin.

In the static-lattice approximation, the chemical potential at bilayer condensation is $30\text{--}50 \text{ K}$ lower than the value for bulk condensation for the cases listed in Table I. In the harmonic-lattice approximation, the calculated offset is $50\text{--}65 \text{ K}$. The value derived from the LEED isotherms^{64,69} (Sec. III A) is 80 K . We have not treated the possibility of a stable trilayer for $N_2/\text{graphite}$: the frustrated molecular ordering makes it doubtful, but an offset of about 60 K (7%) from the bulk chemical potential is a margin similar to that for the bilayer of $Xe/\text{Ag}(111)$, where model calculations⁵⁶ do show a stable trilayer.

B. Discussion

The main observational support for monolayer pinwheel ordering in $N_2/\text{graphite}$ is the fitting by Wang *et al.*¹⁴ of neutron-diffraction data for the dense monolayer. Diffraction data for a mixture of argon and carbon monoxide on graphite⁸⁰ are consistent with pinwheel ordering and nuclear magnetic-resonance data for ortho- H_2 on graphite⁸¹ at temperatures below 0.6 K are interpreted

as showing pinwheel ordering. Our calculations for N_2 /graphite show, in six of the eight cases (sometimes, by extrapolation), at least a small chemical-potential range where there is a stable monolayer pinwheel.

The results are sensitive to the interaction models, because the stability margins in chemical potential are only of the order of 10 K for several-bilayer structures. We felt compelled to give a treatment which included the approximate 150 K per molecule of zero-point energy because it might have changed the relative stability of structures differing by 5–8 % in area per molecule; that did not occur in this work.

Dynamical instabilities (i.e., negative eigenvalues of the dynamical matrix) arose at several stages of the calculations. The instability for the $(\sqrt{3} \times \sqrt{3})R30^\circ$ commensurate monolayer herringbone was simply a consequence of using an incomplete interaction model, and was removed by including the quadrupole terms in the dynamical matrix. The instability for the monolayer pinwheel could be moved out of the thermodynamic stability range by dropping electrostatic screening (image) terms from the model; such a step was necessary for the modeling of CO/graphite,^{50,51} but here it has the consequence of also eliminating the only bilayer with a triangular center-of-mass lattice.

The quasiharmonic approximation for the thin molecular layers is more problematical than for inert-gas bilayers and trilayers.^{25,56} Failures of the approximation, notably the marked lowering of calculated frequencies for configurations in the vicinity of dynamically unstable states, draw searches for the minimum free-energy structure into nonphysical domains. The extreme case is the bilayer pinwheel, where it is difficult to find a starting set of parameters for the search which correspond to a dynamically stable structure. The quasiharmonic free energy in its full variational form, with the fourth-order anharmonicity included,⁸² might remove this problem, but evaluating the extra term would significantly lengthen the calculation.

Kuchta and Etters²³ find bilayers with a character which changes with lattice constant from bilayer herringbone to bilayer pinwheel, with an intermediate structure which has a herringbone first layer and pinwheel second layer. Since their unit cells are (slightly) oblique, symmetry does not require a succession of phase changes. Two features of our calculations are consistent with their progression: (1) the bilayer pinwheel becomes dynamically unstable with increasing area (but, apparently in the second layer), and (2) an incommensurate bilayer herringbone becomes unstable with decreasing area, for a wave vector at the corner of the Brillouin zone corresponding to a doubling of the planar unit cell from the 2×1 herringbone to the 2×2 pinwheel cell (and with dominant motion in the second layer).

For a measure of the zero-point librations, we calculated the mean-square libration amplitude at 0 K, using Eq. (2.12) and the $X1$ model without images. The root-mean-square angular deviations are the following: 15.6° in the $Pa3$ lattice ground state, 18° in the commensurate herringbone monolayer, 23° and 16° for the pin and wheel molecules, respectively, in the monolayer pinwheel at

$14.1 \text{ \AA}^2/\text{molecule}$, 16° and 21° for molecules in the first and second layers, respectively, of the uniaxially incommensurate bilayer herringbone at $7.40 \text{ \AA}^2/\text{molecule}$, and, for the bilayer pinwheel at $6.89 \text{ \AA}^2/\text{molecule}$, 22° and 16° for the pin and wheel molecules, respectively, in the first layer, and 18° for the second-layer molecules. Thus the librations are larger in the adsorbed layer than in the bulk; the harmonic-lattice approximation is likely to be less accurate for the adsorbed layer. The values for the bilayer pinwheel run counter to the result for the eigenvectors of unstable modes, where the dominant entry is the amplitude for the second-layer pin molecule. For the monolayer herringbone, the molecular-dynamics spectra of Tildesley and Lynden-Bell²⁸ are in good agreement with the harmonic frequencies.

The mean-square displacement of the center of mass of the incommensurate monolayer is divergent for lateral (x and y) displacements, as is the case for monatomics. In particular, we verified this, using Eq. (2.12), for the uniform uniaxially incommensurate monolayer herringbone.

V. CONCLUDING REMARKS

Calculations with a realistic potential model which include zero-point energy terms reproduce the energies and lengths of the observed monolayer phases of nitrogen adsorbed on graphite. For six of the eight cases treated, there is evidence for a dense triangular monolayer lattice of the centers of mass with lattice constants in the range observed in LEED and in neutron diffraction. We differ from Kuchta and Etters²³ in finding a chemical potential range where this pinwheel structure is stable relative to the monolayer herringbone and to the bilayer; however, the stability margins are small, as they noted, and are sensitive to details of the interaction models. We differ from You and Fain⁶³ in assigning pinwheel rather than 2-out herringbone ordering to the triangular lattice: this contradiction is troubling, because You and Fain based their assignment on a glide-plane symmetry which is absent from the pinwheel, and because our searches for 2-out herringbone structures led to no viable candidates.

Similarly, we have examined two classes of bilayer structures, the herringbone and pinwheel. Both electron¹⁰- and neutron¹⁴-diffraction data indicate that the center-of-mass lattice is nearly triangular. We find a dense bilayer herringbone with a centered rectangular lattice for the centers of mass which has an aspect ratio 10% from the $\sqrt{3}$ of the triangular lattice. This feature is insensitive to details of our modeling and is characteristic of the dense packing of the linear molecules.

The use of harmonic-lattice dynamics for α - N_2 has been criticized because of the relatively large zero-point librational amplitudes. The zero-point librational amplitudes are even larger for the thin layers of N_2 /graphite. The quasiharmonic theory does treat some of the cases and then leads to absolute free energies and chemical potentials. Cases which have not been directly treated here may be reached by thermodynamic constructions based on these cases and the use of computer simulations.

ACKNOWLEDGMENTS

This work was supported in part by the National Science Foundation through Grants No. DMR-85-16116 and No. DMR-88-17761 and by a grant of computer time from the San Diego Supercomputer Center. One of us

(S.E.R.) was also supported in part with funds provided by U.S. Department of Education Award No. P200A80214. This paper is based on a Ph.D. thesis submitted by the same coauthor (S.E.R.) in partial fulfillment of the requirements for the Doctor of Philosophy degree, University of Wisconsin–Madison.

- *Present address: Department of Mathematics, Texas A&M University, College Station, Texas 77843.
- ¹N. G. Parsonage and L. A. K. Staveley, *Disorder in Crystals* (Clarendon, Oxford, 1978).
- ²R. W. G. Wyckoff, *Crystal Structures* (Interscience, New York, 1963), Vol. 1, p. 30.
- ³J. L. Seguin, J. Suzanne, M. Bienfait, J. G. Dash, and J. A. Venables, *Phys. Rev. Lett.* **51**, 122 (1983).
- ⁴H. M. James, *Phys. Rev.* **167**, 862 (1968); *Phys. Rev. B* **2**, 2213 (1970).
- ⁵T. T. Chung and J. G. Dash, *Surf. Sci.* **66**, 559 (1977).
- ⁶A. D. Migone, H. K. Kim, M. H. W. Chan, J. Talbot, D. J. Tildesley, and W. A. Steele, *Phys. Rev. Lett.* **51**, 192 (1983).
- ⁷Q. M. Zhang, H. K. Kim, and M. H. W. Chan, *Phys. Rev. B* **33**, 413 (1986).
- ⁸Q. M. Zhang, H. K. Kim, and M. H. W. Chan, *Phys. Rev. B* **32**, 1820 (1985).
- ⁹Y. Larher, *J. Chem. Phys.* **68**, 2257 (1978).
- ¹⁰R. D. Diehl and S. C. Fain, Jr., *Surf. Sci.* **125**, 116 (1983).
- ¹¹J. K. Kjems, L. Passell, H. Taub, J. G. Dash, and A. D. Novaco, *Phys. Rev. B* **13**, 1446 (1976).
- ¹²J. Eckert, W. D. Ellenson, J. B. Hastings, and L. Passell, *Phys. Rev. Lett.* **43**, 1329 (1979).
- ¹³R. Wang, S.-K. Wang, H. Taub, J. C. Newton, and H. Schechter, *Phys. Rev. B* **35**, 5841 (1987).
- ¹⁴S.-K. Wang, J. C. Newton, R. Wang, H. Taub, J. R. Dennison, and H. Schechter, *Phys. Rev. B* **39**, 10 331 (1989).
- ¹⁵K. Morishige, C. Mowforth, and R. K. Thomas, *Surf. Sci.* **151**, 289 (1985).
- ¹⁶M. Nielsen, K. Kjaer, J. Bohr, and J. P. McTague, *J. Electron Spectrosc. Relat. Phenom.* **30**, 111 (1983).
- ¹⁷D. A. Goodings and M. Henkelman, *Can. J. Phys.* **49**, 2898 (1971).
- ¹⁸J. K. Kjems and G. Dolling, *Phys. Rev. B* **11**, 1639 (1975).
- ¹⁹B. C. Kohin, *J. Chem. Phys.* **33**, 882 (1960).
- ²⁰W. A. Steele, A. V. Vernov, and D. J. Tildesley, *Carbon* **25**, 7 (1987).
- ²¹C. Peters and M. L. Klein, *Phys. Rev. B* **32**, 6077 (1985).
- ²²L. W. Bruch, *J. Chem. Phys.* **79**, 3148 (1983).
- ²³B. Kuchta and R. D. Ethers, *Phys. Rev. B* **36**, 3400 (1987).
- ²⁴B. Kuchta and R. D. Ethers, *Phys. Rev. B* **36**, 3407 (1987).
- ²⁵L. W. Bruch and M. S. Wei, *Surf. Sci.* **100**, 481 (1980).
- ²⁶C. R. Fuselier, N. S. Gillis, and J. C. Raich, *Solid State Commun.* **25**, 747 (1978).
- ²⁷G. Cardini and S. F. O'Shea, *Surf. Sci.* **154**, 231 (1985).
- ²⁸D. J. Tildesley and R. M. Lynden-Bell, *J. Chem. Soc. Faraday Trans. (II)* **82**, 1605 (1986); R. M. Lynden-Bell (private communication).
- ²⁹S. F. O'Shea and M. L. Klein, *Phys. Rev. B* **25**, 5882 (1982); *Chem. Phys. Lett.* **66**, 381 (1979).
- ³⁰L. W. Bruch, *Surf. Sci.* **125**, 194 (1983).
- ³¹J. O. Hirschfelder, C. F. Curtiss, and R. B. Bird, *Molecular Theory of Gases and Liquids* (Wiley, New York, 1964), Sec. 13.4.
- ³²R. Berns and A. van der Avoird, *J. Chem. Phys.* **72**, 6107 (1980).
- ³³F. Visser, P. E. S. Wormer, and P. Stam, *J. Chem. Phys.* **79**, 4973 (1983).
- ³⁴F. D. Medina and W. B. Daniels, *J. Chem. Phys.* **64**, 150 (1976), and references contained therein.
- ³⁵M. S. H. Ling and M. Rigby, *Mol. Phys.* **51**, 855 (1984).
- ³⁶R. D. Ethers, V. Chandrasekharan, E. Uzan, and K. Kobashi, *Phys. Rev. B* **33**, 8615 (1986).
- ³⁷B. Kuchta and T. Luty, *J. Chem. Phys.* **78**, 1447 (1983); T. Luty, A. van der Avoird, and R. M. Berns, *J. Chem. Phys.* **73**, 5305 (1980).
- ³⁸N. Corbin, W. J. Meath, and A. R. Allnatt, *Mol. Phys.* **53**, 225 (1984).
- ³⁹C. S. Murthy, K. Singer, M. L. Klein, and I. R. McDonald, *Mol. Phys.* **41**, 1387 (1980).
- ⁴⁰C. S. Murthy, S. F. O'Shea, and I. R. McDonald, *Mol. Phys.* **50**, 531 (1983).
- ⁴¹J. Talbot, D. J. Tildesley, and W. A. Steele, *Faraday Discuss. Chem. Soc. (London)* **80**, 91 (1985); J. Talbot, D. J. Tildesley, and W. A. Steele, *Surf. Sci.* **169**, 71 (1986).
- ⁴²A. Vernov and W. A. Steele, *Surf. Sci.* **171**, 83 (1986); V. R. Bhethanabotla and W. A. Steele, *J. Chem. Phys.* **91**, 4346 (1989).
- ⁴³P. A. Monson and M. Rigby, *Mol. Phys.* **39**, 1163 (1980); **42**, 249 (1981).
- ⁴⁴C. Graham, J. Pierrus, and R. E. Raab, *Mol. Phys.* **67**, 939 (1989).
- ⁴⁵K. C. Ng, W. J. Meath, and A. R. Allnatt, *Mol. Phys.* **33**, 699 (1977).
- ⁴⁶W. A. Steele, *J. Phys. (Paris) Colloq.* **38**, C4-61 (1977).
- ⁴⁷W. A. Steele, *Surf. Sci.* **36**, 317 (1973).
- ⁴⁸Y. P. Joshi and D. J. Tildesley, *Mol. Phys.* **55**, 999 (1985).
- ⁴⁹A. D. McLachlan, *Mol. Phys.* **7**, 381 (1964).
- ⁵⁰J. Belak, K. Kobashi, and R. D. Ethers, *Surf. Sci.* **161**, 390 (1985).
- ⁵¹C. Peters and M. L. Klein, *Mol. Phys.* **54**, 895 (1985).
- ⁵²S. Rauber, J. R. Klein, M. W. Cole, and L. W. Bruch, *Surf. Sci.* **123**, 173 (1982).
- ⁵³H.-Y. Kim, M. W. Cole, F. Toigo, and D. Nicholson, *Surf. Sci.* **198**, 555 (1988).
- ⁵⁴G. R. Alms, A. K. Burnham, and W. H. Flygare, *J. Chem. Phys.* **63**, 3321 (1975).
- ⁵⁵W. J. Briels, A. P. J. Jansen, and A. van der Avoird, *Adv. Quantum Chem.* **18**, 131 (1986).
- ⁵⁶L. W. Bruch and X.-Z. Ni, *Faraday Discuss. Chem. Soc. (London)* **80**, 217 (1985).
- ⁵⁷D. J. Chadi and M. L. Cohen, *Phys. Rev. B* **8**, 5747 (1973).
- ⁵⁸S. L. Cunningham, *Phys. Rev. B* **10**, 4988 (1974).
- ⁵⁹S. E. Roosevelt, Ph.D. thesis, University of Wisconsin–

- Madison, 1989 (unpublished).
- ⁶⁰T. A. Scott, Phys. Rep. **27C**, 89 (1976).
- ⁶¹R. D. Diehl, M. F. Toney, and S. C. Fain, Jr., Phys. Rev. Lett. **48**, 177 (1982).
- ⁶²R. D. Diehl and S. C. Fain, Jr., Phys. Rev. B **26**, 4785 (1982).
- ⁶³H. You and S. C. Fain, Jr., Faraday Discuss. Chem. Soc. (London) **80**, 159 (1985).
- ⁶⁴R. D. Diehl and S. C. Fain, Jr., J. Chem. Phys. **77**, 5065 (1982).
- ⁶⁵R. LeSar, J. Chem. Phys. **81**, 5104 (1984).
- ⁶⁶M. J. Bojan and W. A. Steele, Langmuir **3**, 116 (1987).
- ⁶⁷J. Piper, J. A. Morrison, C. Peters, and Y. Ozaki, J. Chem. Soc. Faraday Trans. (I) **79**, 2863 (1983), and references contained therein.
- ⁶⁸R. D. Diehl, C. G. Shaw, S. C. Fain, Jr., and M. F. Toney, in *Ordering in Two Dimensions*, edited by S. K. Sinha (North-Holland, New York, 1980) p. 199.
- ⁶⁹This avoids the problems of calibrating the LEED thermodynamics to the higher-temperature nitrogen vapor-pressure measurements [S. C. Fain (private communication)].
- ⁷⁰A. B. Harris and A. J. Berlinsky, Can. J. Phys. **57**, 1852 (1979).
- ⁷¹A. B. Harris, O. G. Mouritsen, and A. J. Berlinsky, Can. J. Phys. **62**, 915 (1984).
- ⁷²O. G. Mouritsen and A. J. Berlinsky, Phys. Rev. Lett. **48**, 181 (1982).
- ⁷³R. M. Lynden-Bell, J. Talbot, D. J. Tildesley, and W. A. Steele, Mol. Phys. **54**, 183 (1985).
- ⁷⁴A. Vernov and W. A. Steele, Langmuir **2**, 219 (1986).
- ⁷⁵R. D. Etters, in *Simple Molecular Systems at Very High Density*, edited by A. Polian, P. Loubeyre, and N. Boccara (Plenum, New York, 1989).
- ⁷⁶K. Kobashi and R. D. Etters, J. Chem. Phys. **82**, 4341 (1985).
- ⁷⁷F. Y. Hansen, V. L. P. Frank, H. Taub, L. W. Bruch, H. J. Lauter, and J. R. Dennison, Phys. Rev. Lett. **64**, 764 (1990).
- ⁷⁸G. Cardini and S. F. O'Shea, Phys. Rev. B **32**, 2489 (1985).
- ⁷⁹C. Peters and M. L. Klein, Faraday Discuss. Chem. Soc. **80**, 199 (1985).
- ⁸⁰H. You, S. C. Fain, Jr., S. Satija, and L. Passell, Phys. Rev. Lett. **56**, 244 (1986).
- ⁸¹P. R. Kubik, W. N. Hardy, and H. Glattli, Can. J. Phys. **63**, 605 (1985).
- ⁸²M. S. Wei and L. W. Bruch, J. Chem. Phys. **75**, 4130 (1981).

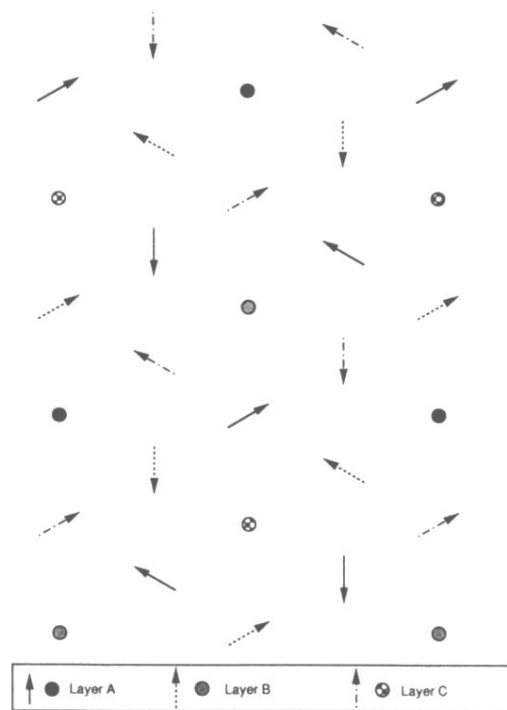


FIG. 1. Two-dimensional projection of layer stacking along the (111) axis of the $Pa\bar{3}$ lattice. The stacking sequence is ABC . Circles denote molecular axes oriented perpendicular to the plane and arrows indicate the orientations of projections of molecular axes onto the plane.